International Journal of Education and Science Research Review
E-ISSN 2348-6457
Volume-6, Issue-2, April - 2019
P-ISSN 2349-1817
www.ijesrr.org
Email- editor@ijesrr.org

Offshore Wind Farm Low-Frequency Alternating-Current Uncontrolled Rectification

Dr. Mahendra Kumar
Guru Kashi University, Talwandi Sabo

ABSTRACT

The advantages of an HVDC transmission system are discussed alongside the constraints of an A transmission system over large distances. An offshore wind farm with turbines fitted with full range converters is part of the power system under investigation. A local AC grid serves as the collection network. The HVDC system is used to transmit power. Offshore wind farm integration with the main electricity system is a key concern. HVAC, Line commutated HVDC, and voltage source based HVDC are all options for transporting electricity from wind farms (VSCHVDC). In this study, a Low Frequency AC (LFAC) transmission system is utilised to interconnect offshore wind farms to improve transmission capabilities, as well as a DC collecting system with series connected wind turbines to decrease cabling requirements at the offshore. To demonstrate the system's performance, simulations are run in MATLAB/SIMULINK.

***Index Terms*—Power Transmission, Thyristor Converters, Underwater Power Cables, Wind Energy**

I. INTRODUCTION

The growing popularity and eventual need of employing renewable energy sources such as wind, solar, and hydropower has resulted in significant economic and technological innovation and progress. Because of the greater space available and superior wind energy potential in offshore areas, offshore wind farms are likely to play a big role in future electric generation. Power engineers are particularly interested in the connectivity and transmission of renewable resources into synchronous grid networks. Because switching systems may readily provide good controllability of electrical signals such as changing voltage and frequency levels, and power factors, switching systems have been employed for resilient and dependable transmission and connectivity of renewable energy into central grid systems. High-voltage ac (HVAC) and high-voltage dc (HVDC) are well-known transmission systems today [1-3]. HVAC transmission is advantageous since the protection system and changing voltage levels using transformers are very simple to construct. However, due to the large capacitance of submarine ac power cables, the considerable charging current lowers the active power transmission capacity and restricts the transmission distance.

II. POWER SYSTEM DETAILS

The system under investigation consists of a 50-turbine wind farm with an MVA rating of 3.6MV A for each turbine. As a result, the wind farm's MVA rating is 180MV A. For variable speed operation, turbines use induction generators and back-to-back full range voltage source converters (VSC). Variable speed wind turbines with back-to-back full-range voltage source converters (VSC) provide the following advantages: (a) Power optimization, e.g., getting higher power production at varying wind speeds; and (b) Mechanical load reduction, resulting in lower maintenance costs. It is also feasible to have independent variable speed for each wind turbine in the wind farm based on the available wind at that particular wind turbine using this turbine configuration with induction generator and back-to-back full-range converters. The wind dispersion is not uniform for all wind turbines in a big wind farm. Figure 1 shows a diagram of the wind turbine components, which is explored in depth in [4].

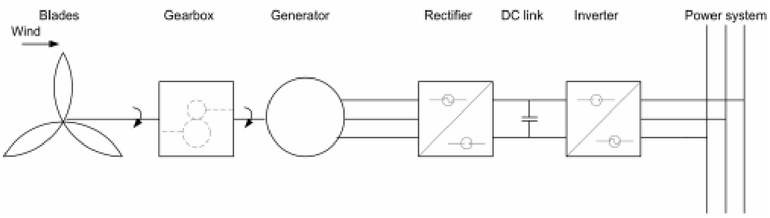

Fig. 1. Wind turbine components layout.

All turbines are connected to a 33kV AC collector network in a typical wind farm arrangement. On the offshore location, a park transformer elevates the collector network voltage to 100kV. The collecting network wires are simulated using a lumped equivalent model. A HVDC link connects the wind farm to the on-land AC grid/pcc, with a rectifier VSC present at the offshore platform and an inverter VSC present on-land. The multilayer voltage source converters are regulated at each end such that under typical operating conditions, 100 percent of the wind farm's power is supplied to the grid.

In the next sections, we'll go through the specifics of the control strategy. With two poles at 100kV, a 100km DC bipolar transmission is explored. Figure 2 illustrates the system's schematic diagram.

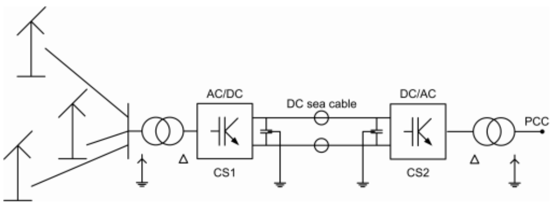

Fig. 2. Schematic connection of wind farm to the on-land grid.

III. SYSTEM CONFIGURATION AND CONTROL

A medium-voltage dc collecting bus is established at the receiving end by rectifying the ac output power of series-connected wind turbines. The entire power provided by the wind turbines is represented by a dc current source Iw. To convert dc electricity to low-frequency (20-Hz) ac power, a dc/ac 12-pulse thyristor-based inverter is employed. It's linked to a three-winding transformer, which boosts the voltage for transmission. The 11th, 13th, and higher-order (23rd) current harmonics are suppressed by AC filters, which also provide reactive power to the converter.

3.1. Sending-End Control

Figure 3 depicts the sending-end inverter's control arrangement. The voltage at the inverter terminals is adjusted by the controller to manage the dc bus voltage. The firing angle is determined using the cosine wave crossing approach.

$$\alpha_S = \arccos\left(\frac{V^*}{V_P}\right) \tag{1}$$

Where V_p is the peak value of the cosine wave Note that $V^*<0$ and $90^0<\alpha_s<180^0$(using common notation), since the converter is in the inverter mode of operation. V and V_s (line-to-neutral, rms) are related by

$$V = \frac{6\sqrt{6}V_S}{\pi n_S}\cos\left(\alpha_S\right) \tag{2}$$

A phase-locked loop (PLL) provides the angular position of the ac-side voltage, which is necessary for generating the firing pulses of the thyristors. It also outputs the rms value of the

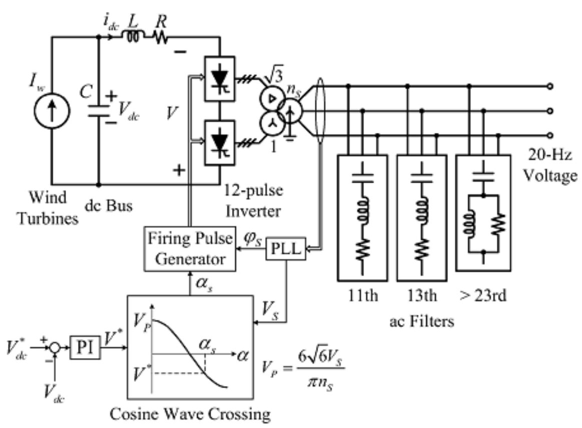

Fig. 3. Sending-end inverter control

Fundamental component of the voltage, which is used in the firing-angle calculation.

3.2. Receiving-End Control

Figure 4 shows the construction of the cycloconverter controller at the receiving end. The control goal is to maintain a constant 20-Hz voltage 1 of a certain rms value V*cyc at all times (line-to-neutral). The signal conditioning logic represented in Fig. 5 is used to get the fundamental component of the cycloconverter voltage Vcyc. As demonstrated in Fig. 6, which employs phase-a as an example, the firing angles are computed using the cosine wave crossing approach. The phase-a positive and negative converters (labelled "aP" and "aN" in Fig.3) have firing angles of and, respectively. The average voltage at the 20-Hz terminals of the optimistic converter is given by

$$V_{aP} = \frac{3\sqrt{6}V_G}{\pi n_R}\cos(\alpha_{aP}) \tag{3}$$

Where V_G the rms is value of the line-to-neutral voltage at the grid side, and n_R is the turn's ratio of the transformers. The condition $\alpha_a p+\alpha_a N=\pi$ ensures that average voltages with the same polarity are generated from the positive and negative converter at the 20-Hz terminals. The firing pulses $S_a p$ and $S_a N$ are not simultaneously applied to both converters, in order to obtain a non circulating current mode of operation. This functionality is embedded in the "Bank Selector" block of Fig. 4, which operates based on the filtered current $i_{cyc,abc}$. Note (for later use) that the maximum line-to-neutral rms value of the 20-Hz cycloconverter voltage.

$$V_{\mathrm{cyc}}^{\max} = \frac{3\sqrt{3}V_G}{\pi n_R} \tag{4}$$

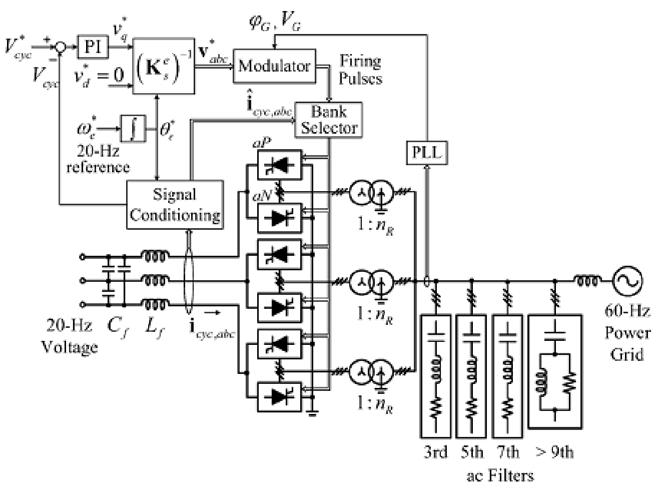

Fig. 4. Receiving-end cycloconverter control. (The reference frame transformation matrix is defined in, and transforms variables from the stationary to the synchronous reference frame.)

And that a voltage ratio is defined as

$$r = \frac{V_{\text{cyc}}}{V_{\text{cyc}}^{\max}}. \tag{5}$$

In practice, the theoretical maximum value 1 cannot be achieved, due to the leakage inductance of the transformers, which was ignored in the analysis.

IV. SYSTEM DESIGN

4.1. Main Power Components

The primary power components are chosen based on a steady-state study of the LFAC transmission system (see Figure 3) and the following assumptions:

• The reactor, thyristors, filters, and transformers all have power losses that are disregarded.

• Transformer resistances and leakage inductances are ignored.

•An analogous capacitance corresponding to the fundamental frequency is then used to represent filters.

• The plan is based on the expected operating circumstances (i.e., maximum power output).

The average value of the dc current Idc equals Iw in the steady state, hence the power provided by wind turbines is Iw.

$$P_w = V_{\text{dc}} I_w. \tag{6}$$

For the 12-pulse converter, the rms value of the current at the transmission side is

$$I = \frac{2\sqrt{6}}{\pi} \frac{I_w}{n_S}. \tag{7}$$

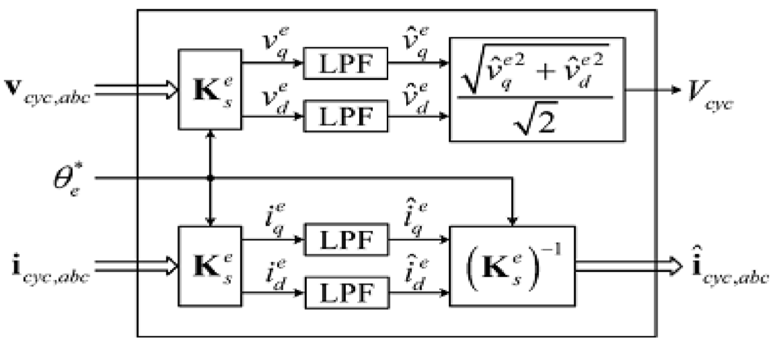

Fig. 5. Details of the signal conditioning block. (LPF first-order low-pass filters, with time constants equal to 0.05 s and 0.01 s for the voltage and current, respectively.)

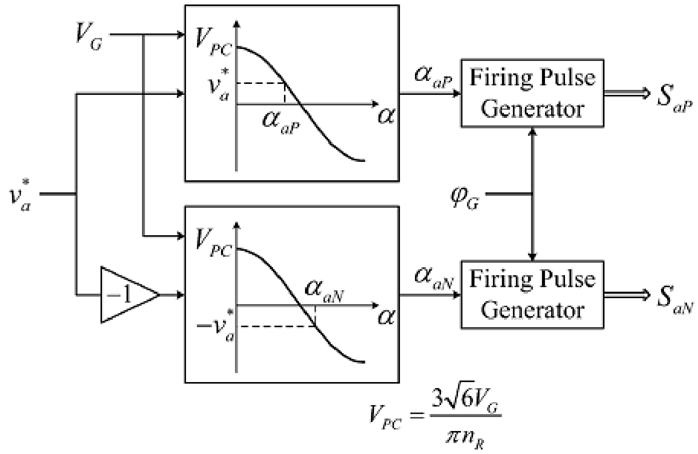

Fig. 6. Modulator for phase a.

Hence, (7) can be written a

$$I = MP_w \tag{8}$$

With

$$M = \frac{2\sqrt{6}}{\pi n_S V_{dc}} \tag{9}$$

Let $\hat{V}_s$= Vs∟0^0 $\hat{i}$ and denote the phasors of the line-to neutral voltage and line current, respectively. Since -$\hat{I}$ lags $\hat{V}$ by α [28], it follows that $\hat{I} = I\angle 180^\circ - \alpha_S$. The active power delivered by the 12-pulse inverter is given by

$$P_S = P_w = 3V_S I\cos(\alpha_S - 180^\circ) = -3V_S I\cos(\alpha_S) > 0. \tag{10}$$

Substitution of (8) into (10) yields

$$\cos(\alpha_S) = -\frac{1}{3MV_S} \tag{11}$$

And

$$\sin(\alpha_S) = \sqrt{1 - \frac{1}{9M^2V_S^2}}. \tag{12}$$

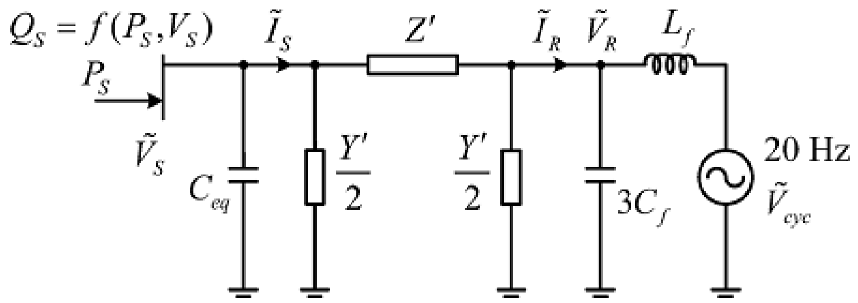

Fig. 7. Equivalent circuit of the LFAC transmission system at fundamental Frequency.

The reactive power generated from the 12-pulse inverter is

$$Q_S = 3V_S I \sin(\alpha_S - 180^\circ) = -3V_S I \sin(\alpha_S) \tag{13}$$

From (10)–(13), it follows that:

$$Q_S = P_S \tan(\alpha_S) = -P_S \sqrt{9M^2 V_S^2 - 1}. \tag{14}$$

The negative sign in (13) and (14) indicates that the 12-pulse inverter always absorbs reactive power. Equation (14) shows that Q_s can be expressed as a function Q_s=f (Ps,Vs). Based on the aforementioned analysis, the steady-state single-phase equivalent circuit of the LFAC transmission system is shown in Fig. 6 The equivalent capacitance of the sending-end a filters at the fundamental frequency is C_{eq} .The transmission line is modeled by an II-equivalent (positive-sequence) circuit using lumped parameters. For Z' and Y'/2, the well-known hyperbolic trigonometric formulae are utilised. Given a wind power plant's Prated power rating, the maximum reactive power absorbed by the 12-pulse inverter may be calculated using (14), which produces

$$Q_{\text{rated}} = P_{\text{rated}} \sqrt{3M^2 V_o^2 - 1} \tag{15}$$

Where Vo is the nominal transmission voltage level (line-to-line rms). Here, it is assumed that the sending-end a filters supply the rated reactive power to the inverter. Therefore

$$C_{\text{eq}} = \frac{Q_{\text{rated}}}{\omega_e V_o^2} \tag{16}$$

Where w_e =2π20rad/s. In addition, the apparent power rating of the transformer at the sending end should satisfy

$$S_{tS} > \sqrt{P_{\text{rated}}^2 + Q_{\text{rated}}^2} = \sqrt{3} P_{\text{rated}} M V_o \tag{17}$$

The cycloconverter's voltage ratio r, which is a design parameter, and the 20-Hz side power factor, which may be computed as follows, determine the reactive power capacity of the a filters and the apparent power rating of the transformers on the 60-Hz grid side. The voltage ratings (nominal and maximum voltage), current ratings, and distributed cable characteristics (resistance, inductance, and capacitance per unit length) are all known for a certain transmission cable. It is expected that a power cable is selected to transfer the rated wind power plant power Prated without exceeding the voltage and current ratings of the cable. (The relationship between active power through the cable and maximum transmission distance, given a certain cable, will be discussed later.) For simplicity, it is further assumed that the rms value of line-to-line voltage at both sending and receiving ends is V_o and the current through Z' and L_f is approximately equal to the current rating of the cable I_{rated}. Since the a filters are designed to supply all reactive power to the 12-pulse inverter at the sending end, the reactive power injected into the 20-Hz side of the cycloconverter can be estimated by using

$$Q_{\mathrm{cyc}}^{20} \approx \mathrm{Im}\{Y'\}V_o^2 + \omega_e 3C_f V_o^2 - 3I_{\mathrm{rated}}^2 \mathrm{Im}\{Z'\} - 3I_{\mathrm{rated}}^2 \omega_e L_f \tag{18}$$

Where the first two terms represent the reactive power generated from the cable and the capacitor of the LC filter, and the last two terms represent the reactive power consumed by the cable and the LC filter's inductor. The active power injected into the cycloconverter from the 20-Hz side can be estimated by using

$$P_{\mathrm{cyc}}^{20} \approx P_{\mathrm{rated}} - \mathrm{Re}\{Y'\}V_o^2 - 3I_{\mathrm{rated}}^2 \mathrm{Re}\{Z'\} \tag{19}$$

The cable's power loss is represented by the final two words. The 20-Hz side power factor may be calculated using (18) and (19). (19). Based on the analysis and calculations, the 60-Hz side power factor PF60 at the transformers' grid side terminals may be calculated using the 20-Hz power factor and the voltage ratio r. The apparent power rating of each of the three receiving-end transformers StR must then meet the requirements.

$$S_{tR} > \frac{P_{\mathrm{cyc}}^{20}}{(3)(\mathrm{PF}^{60})} \tag{20}$$

Also, it is assumed that the grid-side a filters is designed to supply the rated amount of reactive power to the cycloconverter.

V. SIMULATION RESULTS

To demonstrate the validity of the proposed LFAC system, simulations have been carried out using Matlab/Simulink and the Piecewise Linear Electrical Circuit Simulation (PLECS) toolbox. The wind power plant is rated at 180 MW, and the transmission distance is 160 km.

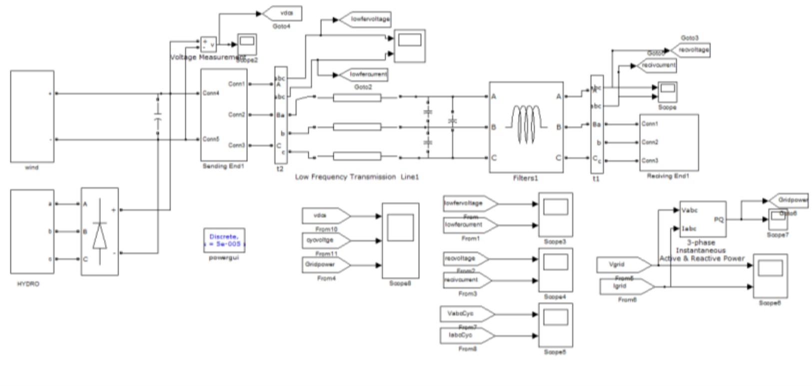

Fig. 8. MATLAB/Simulink model of LFAC transmission system

Figure8 shows the MATLAB/Simulink model of LFAC transmission system.

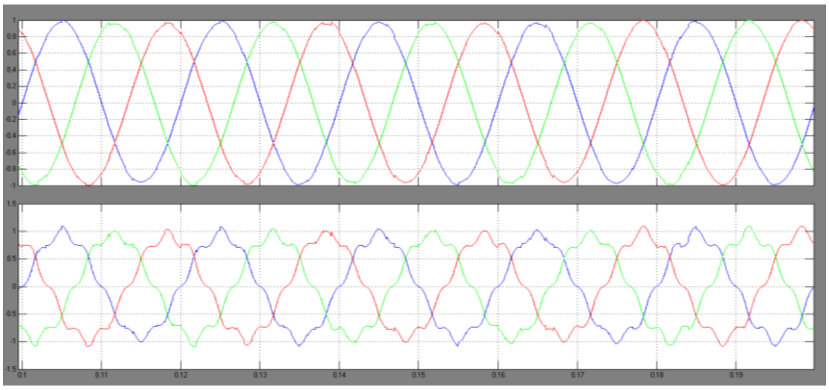

Fig. 9. Simulated voltage and current waveforms sending end

Figure9 shows the simulated voltage and current waveforms sending end

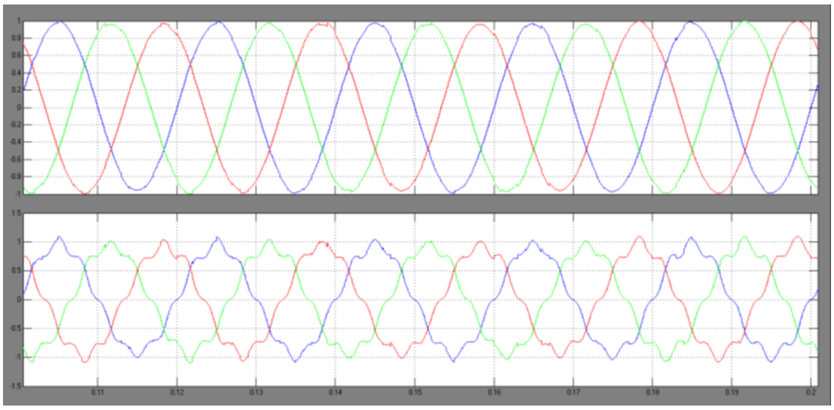

Fig. 10. Simulated voltage and current waveforms receiving end

Figure10 shows the simulated voltage and current waveforms receiving end

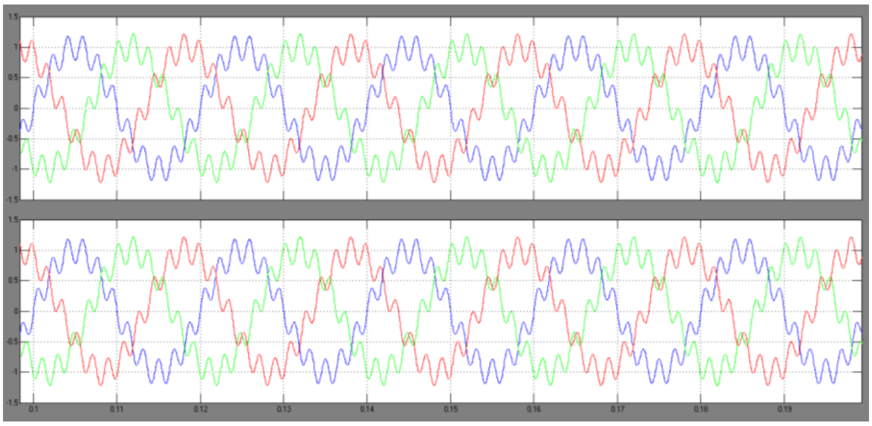

Fig. 11. Simulated voltage and current waveforms Cycloconverter 20-Hz side

Figure11 shows the simulated voltage and current waveforms receiving end

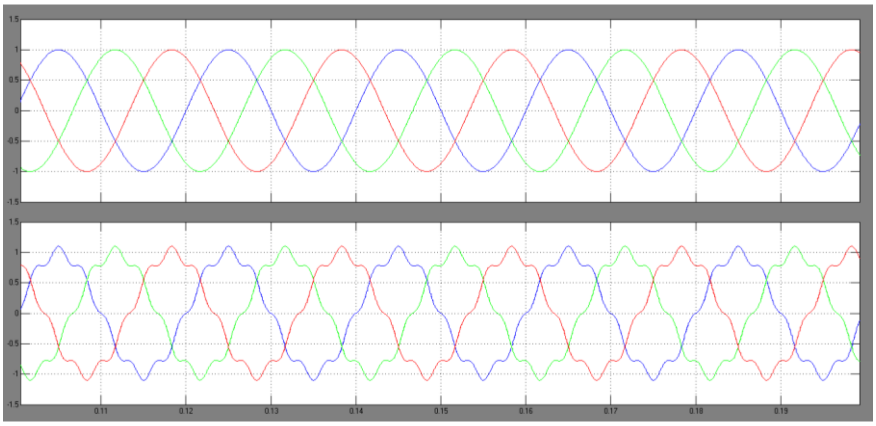

Fig. 12. Simulated voltage and current waveforms 60-Hz power grid side.

Figure12 shows the simulated voltage and current waveforms 60-Hz power grid side.

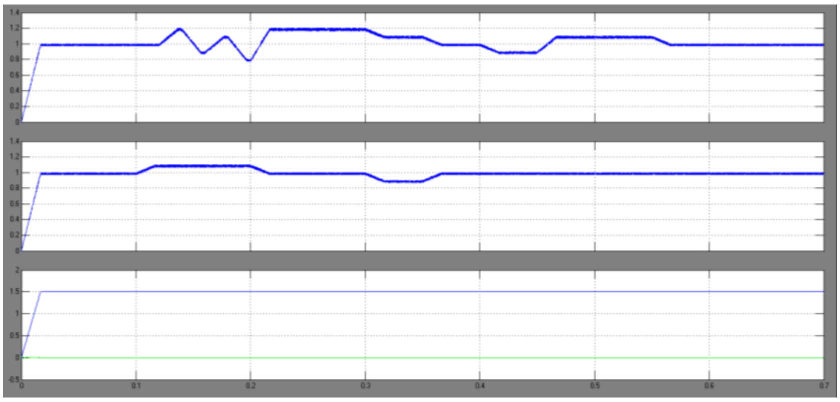

Fig. 13. Transient waveforms during a wind power ramp event.

Figure13 shows the Transient waveforms during a wind power ramp event.

VI.CONCLUSION

For offshore wind generation, a low-frequency ac transmission system has been suggested. It has been explored how to design the system's components and control techniques. Because of the reduced cable charging current, using a low frequency can increase the transmission capabilities of underwater power cables. The suggested LFAC system looks to be a viable option for the long-distance integration of offshore wind power stations, and it might be a good alternative to HVDC systems in some circumstances. Furthermore, establishing a linked low-frequency ac network to transport bulk electricity from several plants would be easier. The main benefit of a wind farm-side VSC control system like this is that turbines with varied generator-converter topologies (for example, induction generators with full range converters and double fed induction generators with partial converters) may be linked to the same VSC platform. The system response and power balance during and outside of grid fault events are shown in the simulation results above.

REFERENCES

[1] National Grid Electricity Transmission, London, U.K., 2011 offshore development information statement, Tech. Rep., Sep. 2011.

[2] T.Mai,R.Wiser,D.Sandor,G.Brinkman,G.Heath,P.Denholm,D. J. Hostick, N. Darghouth, A. Schlosser, and K. Strzepek, "Exploration of high-penetration renewable electricity futures study," National Renewable Energy Laboratory, Golden, CO, Tech. Rep. NREL/TP-6A20-52409-1, National Renewable Energy Laboratory.

[3] N.B.Negra, J.Todorovic, andT. Ackermann, "Loss evaluation of HVAC and HVDC transmission solutions for large offshore wind farms," Elect. Power Syst. Res., vol. 76, no. 11, pp. 916–927, Jul. 2006.

[4] S. Bozhko, G. Asher, R. Li, J. Clare, and L. Yao, "Large offshore DFIG based wind farm with line-commutated HVDC connection to the main grid: Engineering studies, "IEEE Trans. Energy Convers., vol. 23, no. 1, pp. 119–127, Mar. 2008.

[5] O. Gomis-Bellmunt, J. Liang, J. Ekanayake, R. King, and N. Jenkins, "Topologies of multi terminal HVDC-VSC transmission for large offshore wind farms, "Elect. Power Syst. Res., vol. 81, no. 2, pp. 271–281, Feb. 2011.

[6] P. Bresesti, W. L. Kling, R. L. Hendriks, and R. Vailati, "HVDC connection of offshore wind farms to the transmission system, "IEEE Trans. Energy Convers., vol. 22, no. 1, pp. 37–43, Mar. 2007.

[7] S.V.Bozhko, R.Blasco-Giménez, R.Li, J.C.Clare, andG.M.Asher, "Control of offshore DFIG-based wind farm grid with line-commutated HVDC connection,"IEEE Trans. Energy Convers., vol. 22, no. 1, pp. 71–78, Mar. 2007.

[8] J. Arrillaga, High Voltage Direct Current Transmission, 2nd ed. London, U.K.: Institution of Electrical Engineers, 1998.

[9] N. Flourentzou, V. G. Agelidis, and G. D. Demetriades, "VSC-based HVDC power transmission systems: An overview, "IEEE Trans. Power Electron., vol. 24, no. 3, pp. 592–602, Mar. 2009.

[10] T. Funaki and K. Matsuura, "Feasibility of the lower frequency AC transmission," in Proc. IEEE Power Eng. Soc. Winter Meeting, 2000, vol. 4, pp. 2693–2698.

[11] X. Wang, C. Cao, and Z. Zhou, "Experiment on fractional frequency transmission system," IEEE Trans. Power Syst., vol. 21, no. 1, pp. 372–377, Feb. 2006.